Deriving three dimensional reservoir bathymetry from multi-satellite datasets

Augusto Getirana[1,2], Hahn Chul Jung[1,3], Kuo-Hsin Tseng[4,5]

1 NASA Goddard Space Flight Center, Greenbelt, MD, USA

2 Earth System Science Interdisciplinary Center, College Park, MD, USA

3 Science Systems and Applications, Inc., Lanham, MD, USA

4 Center for Space and Remote Sensing Research, National Central University, Taoyuan, Taiwan

5 Institute of Hydrological and Oceanic Sciences, National Central University, Taoyuan, Taiwan

Corresponding author:

Augusto Getirana (augusto.getirana@nasa.gov)

NASA Goddard Space Flight Center

8800 Greenbelt road, Greenbelt, 20771 MD, USA

Abstract

We evaluate different techniques that rebuild reservoir bathymetry by combining multi-satellite imagery of surface water elevation and extent. Digital elevation models (DEMs) are processed in two distinct ways in order to determine 3-D reservoir bathymetry. They are defined as (a) linear extrapolation and (b) linear interpolation. The first one linearly extrapolates the land slope, defining the bottom as the intersection of all extrapolated lines. The second linearly interpolates the uppermost and lowermost pixels of the reservoir's main river, repeating the process for all other tributaries. A visible bathymetry, resulting from the combination of radar altimetry and water extent masks, can be coupled with the DEM, improving the accuracy of techniques (a) and (b). Envisat- and Altika-based altimetric time series is combined to a Landsat-based water extent database over the 2002-2016 period in order to generate the visible bathymetry, and topography is derived from the 3-arcsec HydroSHEDS DEM. Fourteen 3-D bathymetries derived from the combination of these techniques and datasets, plus the inclusion of upstream and downstream riverbed elevations, are evaluated over Lake Mead. Accuracy is measured using ground observations, and show that metrics improve as a function of added data requirement and processing. Best bathymetry estimates are obtained when the visible bathymetry, linear extrapolation technique and riverbed elevation are combined. Water storage variability is also evaluated and shows that best results are derived from the aforementioned combination. This

study contributes to our understanding and representation of reservoir water impoundment impacts on the hydrological cycle.

1. Introduction

Today, water security is a major issue in many regions in the world where humans face a changing climate. Manmade reservoirs and their operation play a key role in water storage and supply, and have a major impact on the water budget at the regional scale (e.g., Wang et al., 2011; Getirana, 2016). Reservoir operation rules or other related information, such as water levels and outflows, are not usually available for large scale modeling purposes. In that sense, numerous studies have proposed different techniques to infer reservoir dynamics worldwide through remote sensing. Water levels are commonly inferred through laser or radar altimetry (Birkett et al., 2010; Cretaux et al., 2011; Okeowo et al., 2017), water extent from land cover imagery, such as Landsat, MODIS and radar images (Messager et al., 2016; Jung et al., 2010; 2011) and storage by combining both of them (Smith & Pavelsky, 2009; Gao et al., 2012; Duan & Bastiaanssen, 2013; Zhang et al., 2014). Other studies have combined water extent with DEMs in order to determine the water storage variability in large river basins (e.g Papa et al., 2013; Cretaux et al., 2015; Salameh et al., 2017).

Hydrological models have been critical in the understanding of the global water availability (e.g., Getirana et al., 2017), but most of these models neglect anthropogenic impacts. Few exceptions represent reservoirs as simple "buckets", where no bathymetric information is required, simulating water multi-use based on generic empirical equations (e.g., Haddeland et al., 2006; Doll et al., 2009). Recent progress in surface water dynamic modeling allows us to obtain a more physically based representation of reservoir operation impacts on the river network system (e.g., Mateo et al., 2014). However, global DEMs, commonly used to derive model parameters, inform us with the surface water elevation rather than the bathymetry, which is defined as the measurement of water body depths. Recent efforts have been put towards the development of more accurate global DEMs, accounting for different sources of errors and interferences (e.g. Yamazaki et al., 2017). Although some studies have suggested ways to improve flow directions in flat DEMs due to floodplains (e.g. Getirana et al., 2009a,b), water bodies are yet to be accurately accounted for in DEM processing. That imposes a major limitation in determining the actual reservoir water volume and depth, their variability and impacts on river systems.

Determining the bathymetry of shallow waters is defined as one of NASA priorities in the 2017-2027 Decadal Survey for Earth Science and Applications from Space for a more accurate representation of the Earth topography (National Academies of Sciences, Engineering, and Medicine, 2017). As a result, accurately representing the impacts of reservoir operation on the surface water dynamics can be achieved with improved DEMs where the bathymetry is properly represented.

Although some studies present techniques to estimate reservoir volume and depth through statistical relationships (e.g., Hollister et al., 2011; Sobek et al., 2011; Heathcote et al., 2015), remotely inferring 3-D reservoir bathymetry has been underexplored. Tseng et al. (2016) introduced a novel methodology to estimate water levels combining water extent time series with a three-dimensional bathymetry obtained through the linear extrapolation of DEMs. The technique was successfully applied to Lake Mead, and results were compared against ground observations. DEM extension through a linear extrapolation is a robust solution providing a first order representation of what the bathymetry could be, and easily transferrable to other reservoirs. However, unless the DEM was acquired during a low water period (Zhang et al., 2016), the inaccuracy of the 3-D bathymetry can be high, since the bottom, defined by the intersection of all extrapolated lines, can be unrealistic.

We address this issue by proposing and comparing different techniques for estimating 3-D reservoir bathymetry exclusively based on satellite data. They can be combined, increasing the level of data requirement and processing. Data sources include the Hydrological data and maps based on SHuttle Elevation Derivatives at multiple Scales (HydroSHEDS; Lehner et al., 2008), Envisat and Altika radar altimeters, and Landsat-based water extents. Lake Mead, located in Nevada, USA, is considered as the study case due to the large ground-based data availability, including bathymetric measurements, used for evaluation. It is also the largest reservoir in the U.S., with a maximum water capacity of 32.2km^3. More specifically, we focus on the lower portion of the lake, the Boulder Basin (see Fig. 1 for location), which has a maximum water capacity of 10.5km^3.

2. Datasets

2.1. Water extent

Water extent time series was derived from Landsat historical datasets (i.e. Landsat 4, 5, and 7 ETM+) for the 1982-2005 period, totaling 585 water extent maps (Tseng et al., 2016). Water pixels were classified from each of the Landsat datasets based on their green and shortwave infrared bands, known as the Modified Normalized Difference Water Index (MNDWI; Xu, 2006). For this study, water masks were generated to include all the pixels that have a value larger than 10% (considered "water") in this Landsat frequency map. The Landsat series has a nominal spatial resolution of 1 arcsec using the WGS84 datum.

2.2. Water level

Water level time series were derived from both satellite and ground observations. We obtained daily historical water elevation from 1983 to 2016 for Lake Mead, at Hoover Dam, from Bureau of Reclamation Records. The water elevations are referenced to the adjusted United States Geological Survey (USGS) datum (i.e. locally known as Power House Datum), 0.55 feet lower than National Geodetic Vertical Datum 1927 (NGVD27) (USDI, 2011). Satellite-based water levels were derived from both Envisat and the SARAL/Altika radar altimeters. Envisat was launched by the European Space Agency (ESA) in 2002 had a cross-track interval ~80km at the Equator and 35-day revisit period, which shared the same orbital elements with preceding ERS-1/-2 missions. The SARAL/Altika launched in February 2013 that follows Envisat is used to extend the altimetry time series. Here, we used the latest version of reprocessed Envisat Sensor Data Record (SGDR V2.1) provided by the *Centre National d'Etudes Spatiales* (CNES) Archiving, Validation, and Interpretation of Satellite Oceanographic data (AVISO) service, corresponding to cycle 6–93. The pass #406 near the Overton Arm of northern Lake Mead (Fig. 1) is selected to retrieved water elevations of both products. Overlapped range between satellite ground track and lake surface is around 3.5km, corresponding to ten 18Hz footprints. A backscattering coefficient threshold is set at 10dB to filter out non-water surfaces with brighter characteristics in radar domain. For Envisat, the ICE-1 range retracker is used to determine the leading-edge position in radar waveforms. Several corrections including the geophysical (solid Earth tide and pole tide), atmospheric (dry/wet troposphere), ionospheric (path delay), and hardware (Ultra Stable Oscillator) terms are further applied to calculate the WGS84 ellipsoidal height.

Envisat time series totals 83 observations, against 24 for SARAL/Altika. Water elevations derived from both satellites were referenced to WGS84 ellipsoid at the overpass near the Overton Arm of northern Lake Mead, covering about ten 18Hz footprints or 3.5km water crossover along track. The root mean square error (RMSE) of bias-corrected Envisat and SARAL/Altika time series is 0.13m and 0.48m, respectively. Combining both time series results in an RMSE of 0.20m. Mean absolute errors (MAE) are 0.18m, 0.51 and 0.29m, respectively.

2.3. Topography and bathymetry

Topography and flow directions were derived from the void-filled HydroSHEDS DEM at 3arcsec, derived from the Shuttle Radar Topography Mission (SRTM; Farr et al. 2007) mission. At the Boulder Basin, a 3arcsec pixel sizes 6940m^2. HydroSHEDS is referenced to both the World Geodetic System 1984 (WGS84) and the Earth Gravitational Model 1996 (EGM96) geoid for horizontal and vertical datum, respectively.

Ground-based bathymetric observations at 1arcsec in the North America Datum 1983 (NAD83) were obtained with USGS. This dataset was acquired in 1999 with a side scan-sonar and chirp seismic reflection survey (USGS, 2003). All generated bathymetric estimates are downscaled at 1arcsec and evaluated against observations. All datasets used in this study (water level time series, topography, and bathymetry) have been corrected to WGS84, before being processed.

3. Methodology

We propose and evaluate 14 experiments resulting from the combination of three bathymetry generation techniques. The techniques are: (i) DEM extrapolation; (ii) DEM interpolation; and (iii) visible bathymetry reconstruction. For both (i) and (ii), DEM is defined as the elevation map, where pixels with constant water surface elevation are masked out. The final bathymetry derived from each procedure replaces the water mask. They are described in the following sections.

3.1. DEM extrapolation

This technique, first proposed in Tseng et al. (2016), defines a conic bathymetry based on the linear extrapolation of the innermost topographic boundary. The window size used to define the slope extrapolation was fixed as 3 pixels, as suggested in Tseng et al. (2016). This procedure can

be applied without additional datasets, only using a DEM, but the bottom of the reservoir can be unrealistic since it is reached when extrapolated lines converge.

3.2. DEM interpolation

This technique requires a hydrologically conditioned DEM and considers that a pixel flows preferentially to one of its eight direct neighbors. As a result, maps of flow directions and drainage area, derived from the DEM, are also needed in order to define the river network. A 9-pixel buffer region is defined along the DEM boundary, guaranteeing a proper selection of elevations upstream the reservoir and downstream the dam. Using the pixels within the buffer, a linear interpolation links the uppermost and lowermost pixels along the main stream of the reservoir, considering the flow directions and upstream drainage. Similar process is repeated for all other tributary streams, and the remaining pixels are filled with interpolated elevations of these rivers. After interpolating all streams crossing the buffer, unfilled pixels within the mask over the reservoir are filled using a moving average window. Based on a sensitivity analysis, we found that the optimal window size for the Boulder Basin is 3 pixels (see Fig. 4). It is important to note that this window size is optimal for this particular case, and may not be ideal for other applications.

In addition to the DEM elevation, in order to further improve the bottom of the reservoir, we also used upstream and downstream riverbed elevation. This information was derived from the ground-based bathymetry. This choice was made because the Boulder Basin's upstream conditions are highly dependent on the operation of the whole Lake Mead system, rather than the naturalized river dynamics. For other cases, more generic solutions could be adopted, such as the use of large-scale empirical equations for the determination of river geometry (e.g. Decharme et al., 2012; Getirana & Paiva, 2013). The use of such equations could facilitate the automation of bathymetry estimation at the global scale, in particular, where observed riverbed elevations are unavailable.

3.3. Visible Bathymetry

An algorithm was developed in order to derive reservoir and lake bathymetry by combining surface water extent and water level time series. The elevation range of the resulting bathymetry will depend on satellite data availability and whether those data were acquired during extreme

wet and dry conditions. Also, accuracy and amount of satellite data will dictate the quality and details provided in the final product. This bathymetry, observable through satellite data, is hereafter called visible bathymetry, or simply VB. The VB algorithm is composed of four sub-steps and a schematic is provided in Fig. 2:

a. Water level and mask time series are combined. Envisat data is linearly interpolated in order to obtain an estimated water level at a given time where Landsat-based water extent is available. At the end of this step, there will be *n* matches of water levels and masks;

b. Water masks are stacked as a function of the elevation. In this sense, water masks are reorganized from the lowest to the highest elevation. Ideally, the water mask at the lowest elevation should also have the smallest extent;

c. Water masks are then corrected based on a consistency test using an occurrence coefficient (c_o): at a given lower water mask layer, the consistency of a *xy* pixel classified as "water" will be verified by counting the number of pixels in higher elevation layers that are also "water". If that number exceeds the c_o threshold, then all tested pixels are classified as "water", otherwise they are all classified as "land". c_o is given as a fraction of xy pixels from that layer to the top layer that is classified as "water", varying from 0 to 1.

d. The bathymetry is then generated by attributing elevations to boundary pixels of all mask layers and using linear interpolation to fill empty spaces between the innermost and outermost boundaries.

3.4. Experimental design

In order to evaluate the accuracy of techniques as a function of their added data requirement and processing, 14 experiments, composed of single procedures or the combination of two or more of them, are evaluated. Processing techniques and datasets composing each experiment are described below and summarized in Table 1:

1. (HS) Bathymetry is simply considered as elevation provided in HydroSHEDS;

2. (I1) Linear interpolation is applied using HydroSHEDS and its corresponding flow direction map;

3. (I2) Linear interpolation is applied using HydroSHEDS and its corresponding flow direction map; upstream riverbed elevation is used for the correction of the uppermost pixel of the main stream to the reservoir in HydroSHEDS;

4. (I3) Linear interpolation is applied using HydroSHEDS and its corresponding flow direction map; upstream and downstream riverbed elevation are used to correct the main stream DEM pixels in HydroSHEDS;

5. (E1) Linear extrapolation is applied using a 3-pixel buffer DEM derived from HydroSHEDS over land;

6. (E2) As E1, but the bottom of the reservoir is constrained by a flat horizontal elevation derived from the downstream riverbed elevation;

7. (E3) As E1, but the bottom of the reservoir is constrained by a surface composed of the linear interpolation between the upstream and downstream riverbed elevations;

8-14. (VHS), (VI1), (VI2), (VI3), (VE1), (VE2) and (VE3) Experiments 1-7 are repeated using HydroSHEDS corrected with visible bathymetry derived from Landsat water extents and Envisat/Altika water level time series.

3.5. Evaluation procedure

The evaluation has been designed to independently test the sensitivity of visible bathymetry parameters, and the fourteen experiments described above. The sensitivity analysis of c_o was performed in order to determine the best visible bathymetry for the Boulder Basin. In this sense, c_o varied from 0 to 1 at incremental steps of 0.1, totaling 11 realizations. The most appropriate c_o value is determined using a tradeoff relationship between accuracy and number of remaining valid pixels composing the visible bathymetry. This tradeoff relationship was chosen rather than an optimization procedure minimizing errors because, as shown in the following section, high c_o values drastically reduce the amount of data used to build the bathymetry.

The bathymetric estimates are evaluated in terms of maximum water storage capacity, V [km^3], average and maximum depths, h_{AVG} and h_{MAX} [m], and relative water storage variability, dV [km^3]. V, h_{AVG} and h_{MAX} were computed using the maximum reported water elevation of 375m for Lake Mead, and dV was derived from ground and satellite water level observations combined with the bathymetries. Bathymetric estimates are also compared against the reference using RMSE, MAE and relative error (RE), and water storage variability with the standard deviation ratio (Stdev ratio). MAE and Stdev ratio are defined as follows:

$$\mathrm{RMSE} = \sqrt{\left[\sum_{i=1}^{np}(x_i - y_i)^2\right]/np} \quad (1)$$

$$\mathrm{MAE} = \sum_{i=1}^{np} \frac{|x_i - y_i|}{np} \quad (2)$$

$$\mathrm{RE} = \frac{\sum_{i=1}^{np} x_i - \sum_{i=1}^{np} y_i}{\sum_{i=1}^{np} y_i} \quad (3)$$

$$\text{Stdev ratio} = \frac{\sigma_s}{\sigma_o} \quad (4)$$

where x and y stand for estimated and observed bathymetric elevations, np is the total amount of pixels composing the bathymetry. σ_s and σ_o represent the standard deviation of estimated and observed water volume time series, respectively.

Water storage is derived from the combination of water level observations with bathymetry estimates. First, the daily ground-based water level time series, assumed as the truth, is combined with bathymetries in order to isolate the impact of water level changes on the water storage. The water storage derived from the reference bathymetry is used as the truth. Then, a fully satellite-based water storage is derived by repeating the same procedure, but using radar altimetry time series.

4. Results and discussion

4.1. Visible bathymetry generation

The experiment using Envisat+Altika data resulted in 253 matches between water level and extent during the 2002-2015 period, with an elevation range of 23.9m, from 329.9m to 353.8m. The longer data availability using gauge-based water levels, from 1983 to 2016, resulted in 584 matches with a wider elevation range, 42.3m from 328.2m to 370.5m.

Results from the sensitivity analysis show that the number of pixels composing VB varies significantly with different c_o values. The least restrictive realization (c_o=0) includes any "water" pixels in all layers, resulting in VBs composed of 50,000 and 112,000 pixels for the Envisat+Altika and gauge-based experiments, respectively. These VBs have large errors, as indicated by the comparison against observations (Biases are -69.2m and -201.3m, and RMSEs are 175.3m and 363m). The performance increases when more restrictive values are used. For example, biases are 3.3m and 1.2m, and RMSEs are 12.1m and 10.7m when c_o=1. The gain in accuracy is counterbalanced by a significant loss of information, with VBs being composed of only 5200 and 4100 pixels, respectively. Fig. 3 shows the relationship between the number of pixels used in VBs and accuracy, as a function of c_o values, for both experiments. It is possible to identify a break in all curves, where the number of pixels significantly drops with low change in accuracy. That break has been identified as c_o=0.5 (marked with circles), where biases are -0.3m and -1.3m, and RMSEs are 10.8m and 11m for the Envisat+Altika and gauge-based experiments, respectively.

4.2. 3-D bathymetry evaluation

Estimates of Boulder Basin bathymetry vary significantly among experiments. As shown in Fig. 5, HydroSHEDS bathymetry (HS) highly underestimates the water storage capacity, as well as average and maximum depths (0.5km^3, 66m and 4m, respectively), when compared to the reference (10.5km^3, 159m and 95m). This result is expected since the bottom of the reservoir is defined in this experiment as the water surface observed by SRTM. This is an indication that using raw DEMs (i.e. no data pre-processing to represent bathymetry over reservoirs) should be avoided. Better bathymetry estimates are obtained with the experiments based on the linear interpolation technique. Fig. 6 shows the differences between estimates and the reference bathymetry, including RMSE and MAE values. When metrics of experiments with and without VB are averaged in different groups, we observe that experiments using the linear interpolation technique (i.e. average of experiments I1, I2, I3, VI1, VI2 and VI3) considerably improves the

accuracy of bathymetry estimates, reducing RMSE and MAE, on average, 40% and 47%, respectively. Among these experiments, if we focus on experiments considering riverbed elevation (i.e. I2, I3, VI2 and VI3), improvements are slightly higher (43% and 50%). The underestimated depths observed upstream the reservoir (upper right corner) in experiments I1 and VI1 are corrected when the linear interpolation is performed using riverbed elevation. Among all experiments using linear interpolation, VI3, considering visible bathymetry and riverbed elevation, resulted in the most accurate volume estimate ($V=7.5km^3$) and average depth ($h_{AVG}=68m$), with RMSE and MAE of 52.3m and 40.5m, respectively. Even though the linear interpolation technique significantly improves the determination of the bottom of the reservoir, a few features are still missing, such as the depressions in the lower left and upper center sides of the reservoir and the elevation in the right side, as shown in Fig. 6. This is likely due to the fact that after interpolating all tributary pixels, the remaining reservoir pixels are not sufficiently explained using a 3x3 moving average with the surrounding interpolated elevations.

The 3-pixel buffer topography applied to HydroSHEDS in the linear extrapolation technique (experiment E1) resulted in a deep reservoir bottom, where all extrapolated lines intersect, highly overestimating V, h_{AVG} and h_{MAX} values ($25.8km^3$, 795m and 234m), and the highest RMSE (208.1m) and MAE (150.5m) values. An enhancement is observed with the inclusion of VB (experiment VE1), with metric values of 170.1m and 112.6m, respectively. However, a significant improvement is noticed when the bathymetry derived from the linear extrapolation technique has its bottom constrained with flat surfaces defined by riverbed elevation. Using the downstream riverbed elevation to derive a flat horizontal reservoir bottom (experiments E2 and VE2) enhances both V and h_{AVG}, and average RMSE and MAE are improved, on average, by 71% and 67%. Using the flat surface defined by the main stream interpolation to constrain the reservoir bottom (experiments E3 and VE3) adds up, improving RMSE and MAE in 69% and 73%, respectively, compared to experiments E1 and VE1.

Adding VB improved bathymetry estimates of all experiments, with RMSE and MAE increasing, on average, 14% and 18%, respectively. The best overall results were obtained from experiments combining VB, linear extrapolation and riverbed elevation. In particular, experiment VI3, using upstream and downstream riverbed elevations, resulted in the most accurate metrics of all

311 experiments, with absolute water volume and average depth of 13.2km^3 and 119.5m, and RMSE
312 and MAE of 44.4m and 32.9m, respectively.

313 **4.3. Water storage variability**

314 If, on one hand, the maximum water storage capacity is highly dependent on the bottom of the
315 reservoir, as discussed above, water storage change reflects how accurate the bathymetry is in the
316 top layer, where water levels vary. Fig. 7a shows bias-removed water volume variability time
317 series, dV, derived from the combination of ground-based water level observations and
318 bathymetry estimates, for the 1983-2016 period. Bias was removed from time series for
319 visualization purposes only, and values are provided for each experiment in the figure.
320 Experiment I1, using the linear interpolation technique, did not perform as well, with higher
321 RMSE (0.6km^3) and lower Stdev ratio (0.59). Both metrics improve with experiments I2 and I3,
322 when riverbed elevation is used, reaching 5.38×10^{-4} km^3 and 0.68, respectively (see Fig. 7 for
323 time series and Table 2 for respective metrics). Although experiments E1 overestimates the
324 maximum water capacity, as described in the previous session, once their biases of 10km^3 are
325 removed, one can notice a high agreement between reference and estimated dV time series, with
326 RMSE values of nearly zero, and Stdev ratio of 1. An overall improvement of all metrics is
327 noticed when VB is considered, with a general improvement of bias, RMSE and Stdev ratio of
328 25%, 119% and 7%, respectively. VB improved Stdev ratio of linear interpolation experiments,
329 but added a minimum deterioration in linear extrapolation experiments. Although adding
330 riverbed elevation to the linear interpolation technique had some improvement on RMSE and
331 Stdev ratio, combining that information with the linear extrapolation technique has not changed
332 these metrics. On the other hand, riverbed elevation significantly impacted biases, with an
333 overall improvement of 51%.

334 Fig. 7b shows bias-removed dV derived from radar altimetry time series combined with
335 bathymetry estimates. Full satellite-based dV is available from 2002 to 2016 at a 35-day
336 repeating cycle, except years 2011 and 2012, corresponding to a gap between Envisat and Altika
337 missions. Results follow the patterns observed when ground-based observations are used.
338 However, the reduced frequency, shorter time series, and error related to the altimeter and
339 algorithms used to derive the water level resulted in a slight difference between metrics derived
340 from each data source. For both ground-based and satellite-based time series, the most accurate

water volume variability time series were obtained with experiment VE3, combining linear extrapolation, riverbed elevation and visible bathymetry, with bias=2.7km^3, RMSE=0 and Stdev ratio=1 for both time series.

5. Summary

This paper presents and compares techniques used to generate 3-D reservoir bathymetry based on remote sensing data. They are composed of three categories that can be coupled, hence increasing levels of data and processing requirements, combining digital elevation models, radar altimetry and land cover maps. DEMs are processed in two distinct ways in order to determine the bathymetry and bottom of the reservoir. They are the (a) linear extrapolation and (b) interpolation. The first one linearly extrapolates land slopes surrounding the reservoir, defining the bottom as the intersection of all extrapolated lines. The second one linearly interpolates pixels beyond the uppermost and lowermost points of the main river of the reservoir, repeating the process for all other tributaries, and filling the remaining pixels with interpolated elevations of these rivers. A partial 3-D bathymetry, called here visible bathymetry, resulting from the combination of radar altimetry and water extent masks, can be coupled to the DEM, improving reservoir bathymetry estimates from (a) and (b). The technique is tested over the Boulder Basin, the lower part of Lake Mead, where ground-based observations are largely available for evaluation. Fourteen experiments with increasing amount of inputs and data processing are evaluated against bathymetric measurements.

In order to determine VB, a parameter called occurrence coefficient c_0 needs to be calibrated. In this sense, a sensitivity analysis is performed and a trade-off approach is used in order to determine the optimal value. c_0 is determined as a function of both RMSE and gain of information in terms of number of pixels used in the generation of the bathymetry map. The optimal value is found somewhere between 0.4 and 0.5, but fixed as 0.5 in this study. It is worth noting that this value is independent of the water level dataset, but it is related to the quality of the water extent maps (e.g. cloud contamination, speckle noise, among other source or errors) and should be carefully reapplied to other cases. At the end of this process, it is assumed that uncertainties intrinsic to the water mask misclassification are minimized, but still present. Errors related to radar altimetry data are also a source of inaccuracy in the proposed algorithm. The average mean absolute error found for the bias-corrected radar altimetry time series is 0.29m,

371 which is one order of magnitude lower than SRTM errors (Farr et al., 2007). Another source of
372 error in this technique is the linear interpolation used to fill the gaps between water boundaries at
373 different elevations. However, that source of error can be minimized, as more data is available.
374 As demonstrated in the sensitivity analysis, errors are still present when using the optimal c_o
375 value.

376 Both interpolation and extrapolation techniques require the definition of window sizes. Here,
377 sizes were defined based on either previous experience, as described in the literature, or on
378 sensitivity tests. Although they were satisfactorily used in both techniques over the Boulder
379 Basin, alternative dimensions might be more appropriate when these techniques are applied to
380 other reservoirs or datasets.

381 The 3-D bathymetry estimates are evaluated in terms of maximum water storage capacity V,
382 average h_{AVG} and maximum h_{MAX} depths, and water storage variability dV. We also use metrics
383 such as bias, RMSE, mean absolute error and standard deviation ratio to determine the accuracy
384 of both bathymetry and dV. Results show that bathymetry estimates combining the linear
385 extrapolation technique, visible bathymetry and riverbed elevation achieved the best accuracy for
386 all selected metrics. Improvements observed using VB with the linear extrapolation technique is
387 likely due to HydroSHEDS's limitations inherited from SRTM DEM errors, which could have a
388 negative impact on slopes. These errors are a function of terrain and land cover characteristics,
389 among others. Additionally, vertical errors can further biased when the DEM is upscaled, and
390 slopes tend to flatten. As a result, it is safe to assume that, in this particular case, VB provides a
391 better estimate of elevations, as opposed to HydroSHEDS.

392 We acknowledge the existence of two limitations in our evaluation. They are: (i) limited number
393 of techniques to generate 3-D bathymetry; and (ii) limited number of evaluation sites. Applying
394 and combining additional extrapolation and interpolation techniques (i.e. polynomial,
395 logarithmic, exponential, among others) to a wider range of reservoirs can result in a more
396 refined evaluation, and metrics could be related to hydrogeological features (e.g. shape, depth,
397 etc.), in order to determine the most appropriate techniques to be used. Unfortunately, access to
398 ground-based bathymetric observations is still limited, restricting a broader evaluation.

The proposed technique is easily transferrable to other reservoirs with the required data availability. In terms of water extent, MODIS-based (Carroll et al., 2017) and Landsat-based (Feng et al., 2016; Pekel et al., 2016) products are readily available globally for a wide timespan. Satellite-based water levels are currently available through the G-REALM (https://www.pecad.fas.usda.gov/cropexplorer/global_reservoir/) and Hydroweb (http://hydroweb.theia-land.fr/) databases at more than 300 lakes and reservoirs globally, and recent developments of automated techniques for time series extraction (e.g. Okeowo et al., 2017) could significantly increase radar altimetry data availability for reservoir monitoring. Radar altimetry data availability is limited to water bodies intersecting satellite tracks and water extent time series acquisition requires extensive data processing, imposing restrictions to a globally automated application of the technique. On the other hand, the linear interpolation combined to riverbed elevation estimates provided competitive results, and could be easily applied globally. Launching in 2021, the future Surface Water and Ocean Topography (SWOT) satellite mission will provide unprecedented information on surface water dynamics, including two-dimensional water level and extent time series. SWOT will considerably improve reservoir monitoring and could be combined with existing datasets towards more accurate bathymetry estimates.

Next steps of this effort include the application of similar procedures to major reservoirs in Africa, such as Lakes Volta, in Ghana, and Nasser, in Egypt, and evaluate their impacts on a hydrological modeling framework. Indeed, refining hydrological model parameters with bathymetry information, as described in this study, will significantly improve the representation and monitoring of anthropogenic impacts on the water cycle at different scales. Ultimately, generating 3-D bathymetry at the global scale will largely benefit the scientific community and refine global databases such as HydroLAKES (Messager et al., 2016).

Acknowledgements

The authors would like to thank the U.S. Bureau of Reclamation (https://www.usbr.gov/) for providing Lake Mead Daily water elevation data. This study was funded by the NASA's Applied Sciences Program - SERVIR.

References

Birkett, C.M., C. Reynolds, B. Beckley, and B. Doorn, From Research to Operations: The USDA Global Reservoir and Lake Monitor, Chapter 2 in 'Coastal Altimetry', eds. S. Vignudelli, A.G. Kostianoy, P. Cipollini, J. Benveniste, Springer Pubs, ISBN 978-3-642-12795-3, 2010.

Carroll, M.L., DiMiceli, C.M., Townshend, J.R.G., Sohlberg, R.A., Elders, A.I., Devadiga, S., Sayer, A.M., Levy, R.C., 2017. Development of an operational land water mask for MODIS Collection 6, and influence on downstream data products. International Journal of Digital Earth, 10(2), 207-218. doi: 10.1080/17538947.2016.1232756.

Cretaux, J.F., Biancamaria, S., Arsen, A., Bergé-Nguyen1 , M., Becker, M., 2015. Global surveys of reservoirs and lakes from satellites and regional application to the Syrdarya river basin. Environmental Research Letters, 10(1) 015002. doi:10.1088/1748-9326/10/1/015002.

Cretaux, J.F., Jelinski, W., Calmant, S., Kouraev, A., Vuglinski, V., Berge-Nguyen, M., Gennero, M.C., Nino, F., Abarca Del Rio, R., Cazenave, A., Maisongrande, P., 2011. SOLS: A lake database to monitor in the Near Real Time water level and storage variations from remote sensing data. Advances in Space Research, 47, 1497–1507. DOI:10.1016/j.asr.2011.01.004

Decharme, B., R. Alkama, F. Papa, S. Faroux, H. Douville, and C. Prigent, 2012: Global off-line evaluation of the ISBA-TRIP flood model. Climate Dyn., 38 (7–8), 1389–1412, doi:10.1007/ s00382-011-1054-9.

Doll, P., Fiedler, K., Zhang, J., 2009. Global-scale analysis of river flow alterations due to water withdrawals and reservoirs. Hydrol. Earth Syst. Sci., 13, 2413–2432.

Duan, Z., Bastiaanssen, W.G.M., 2013, Estimating water volume variations in lakes and reservoirs from four operational satellite altimetry databases and satellite imagery data, Remote Sens. Environ., 134, 403–416, doi:10.1016/j.rse.2013.03.010.

Farr, T. G., and Coauthors, 2007: The Shuttle Radar Topography Mission. Rev. Geophys., 45, RG2004, doi:10.1029/ 2005RG000183.

Feng, Min, Joseph O. Sexton, Saurabh Channan, and John R. Townshend. 2015. "A Global, High-Resolution (30-M) Inland Water Body Dataset for 2000: First Results of a Topographic-Spectral Classification Algorithm." International Journal of Digital Earth. doi:10.1080/17538947.2015.1026420.

Gao, H., C. Birkett, and D. P. Lettenmaier (2012), Global monitoring of large reservoir storage from satellite remote sensing, Water Resour. Res., 48, W09504, doi:10.1029/2012WR012063.

Getirana, A.C.V., and R. C. D. Paiva (2013), Mapping large-scale river flow hydraulics in the Amazon Basin, Water Resour. Res., 49, doi:10.1002/wrcr.20212.

Getirana, A., 2016. Extreme water deficit in Brazil detected from space. Journal of Hydrometeorology, 17(2), 591-599. DOI: 10.1175/JHM-D-15-0096.1.

Getirana, A., Kumar, S., Girotto, M., Rodell, M., 2017. Rivers and floodplains as key components of global terrestrial water storage variability. Geophysical Research Letters, 44. DOI: 10.1002/2017GL074684.

Getirana, A.C.V., Bonnet, M.-P., Martinez, J.-M., 2009a. Evaluating parameter effects in a DEM 'burning' process based on land cover data. Hydrological Processes, 23, 502–514, DOI: 10.1002/hyp.7303.

Getirana, A.C.V., Bonnet, M.-P., Rotunno Filho, O.C., Mansur, W.J., 2009b. Improving hydrological information acquisition from DEM processing in floodplains. Hydrological Processes, 23, 502–514. DOI: 10.1002/hyp.7167.

Haddeland, I., T. Skaugen, and D. P. Lettenmaier, 2006: Anthropogenic impacts on continental surface water fluxes. Geophys. Res. Lett., 33

Heathcote AJ, del Giorgio PA, Prairie YT, Brickman D. 2015. Predicting bathymetric features of lakes from the topography of their surrounding landscape. Canadian Journal of Fisheries and Aquatic Sciences 72:643–650.

Hollister JW, Milstead WB, Urrutia MA. 2011. Predicting Maximum Lake Depth from Surrounding Topography. Schumann GJ-P, editor. PLoS ONE 6:e25764.

Jung, H.C., D. Alsdorf, M. Moritz, H. Lee, and S. Vassolo, Analysis of the relationship between flooding area and water height in the Logone floodplain, Physics and Chemistry of the Earth, 36, 232-240, 2011.

Jung, H.C., J. Hamski, M. Durand, D. Alsdorf, F. Hossain, H. Lee, A. K. M. A. Hossain, K. Hasan, A. S. Khan, and A. K. M. Z. Hoque, Characterization of complex fluvial systems via remote sensing of spatial and temporal water level variations in the Amazon, Congo, and Brahmaputra Rivers, Earth Surface Processes and Landforms, 35, 294-304, 2010.

Lehner, B., Verdin, K., Jarvis, A., 2008. New global hydrography derived from spaceborne elevation data. Eos, Transactions, AGU, 89(10), 93-94.

Mateo, C. M., N. Hanasaki, D. Komori, K. Tanaka, M. Kiguchi, A. Champathong, T. Sukhapunnaphan, D. Yamazaki, and T. Oki (2014), Assessing the impacts of reservoir operation to floodplain inundation by combining hydrological, reservoir management, and hydrodynamic models, Water Reso ur. Res., 50, 7245–7266, doi:10.1002/2013WR014845.

Messager, M.L., Lehner, B., Grill, G., Nedeva, I., Schmitt, O., 2016. Estimating the volume and age of water stored in global lakes using a geo-statistical approach. Nature Communications: 13603. doi: 10.1038/ncomms13603

National Academies of Sciences, Engineering, and Medicine, 2017. Thriving on Our Changing Planet: A Decadal Strategy for Earth Observation from Space. Washington, DC: The National Academies Press. https://doi.org.10.17226/24938.

Okeowo, M., Lee, H., Hossain, F., Getirana, A., 2017. Automated Generation of Lakes and Reservoirs Water Elevation Changes From Satellite Radar Altimetry. Journal of Selected Topics in Applied Earth Observations and Remote Sensing. DOI : 10.1109/JSTARS.2017.2684081

Papa, F., Frappart, F., Güntner, A., Prigent, C., Aires, F., Getirana, A.C.V., Maurer R., 2013. Surface freshwater storage and variability in the Amazon basin from multi-satellite observations, 1993–2007, J. Geophys. Res. Atmos., 118, 11,951–11,965, doi:10.1002/2013JD020500.

Pekel, J.-F., A. Cottam, N. Gorelick, and A. S. Belward (2016), High-resolution mapping of global surface water and its long-term changes, Nature, 540, 418–422, doi:10.1038/nature20584.

Salameh, S., Frappart, F., Papa, F., Güntner, A., Venugopal, V., Getirana, A., Prigent, C., Labat, D., Laignel, B., 2017. 15 years (1993-2007) of surface freshwater storage variability in the Ganges-Brahmaputra river basin using multi-satellite observations. Submitted for publication in Water.

Smith, L.C., Pavelsky, T.M., 2009. Remote sensing of volumetric storage changes in lakes. Earth Surf. Process. Landforms, 34(10), 1353-1358. DOI: 10.1002/esp.1822

Sobek S, Nisell J, Fölster J. 2011. Predicting the depth and volume of lakes from map-derived parameters. Inland Waters 1:177–184.

Tseng, K.H., Shum, C.K., Kim, J.W., Wang, X., Zhu, K., Cheng, X., 2016. Integrating Landsat Imageries and Digital Elevation Models to Infer Water Level Change in Hoover Dam. IEEE Journal of Selected Topics in Applied Earth Observations and Remote Sensing, 9(4), 1696-1709. DOI: 10.1109/JSTARS.2015.2500599

USDI, 2011, Lake Mead area and capacity tables, Boulder Canyon Operations Office, River Operations Group.

USGS, 2003, Mapping the Floor of Lake Mead (Nevada and Arizona): Preliminary Discussion and GIS Data Release U.S. Geological Survey Open File Report 03-320.

Wang, X., C. de Linage, J. Famiglietti, and C. S. Zender (2011), Gravity Recovery and Climate Experiment (GRACE) detection of water storage changes in the Three Gorges Reservoir of China and comparison with in situ measurements, Water Resour. Res., 47, W12502, doi:10.1029/2011WR010534.

Xu, H., 2006, Modification of normalised difference water index (NDWI) to enhance open water features in remotely sensed imagery, Int. J. Remote Sens., vol. 27, pp. 3025–3033.

Yamazaki, D., D. Ikeshima, R. Tawatari, T. Yamaguchi, F. O'Loughlin, J. C. Neal, C. C. Sampson, S. Kanae, and P. D. Bates (2017), A high-accuracy map of global terrain elevations, Geophys. Res. Lett., 44, 5844–5853, doi:10.1002/2017GL072874.

Yamazaki, D., T. Oki, and S. Kanae, 2009: Deriving a global river network map and its sub-grid topographic characteristics from a fine-resolution flow direction map. Hydrol. Earth Syst. Sci., 13, 2241–2251, doi:10.5194/hess-13-2241-2009.

Zhang, S., Foerster, S., Medeiros, P., de Araújo, J.C., Motagh, M., Waske, B., 2016. Bathymetric survey of water reservoirs in north-eastern Brazil based on TanDEM-X satellite data. Science of the Total Environment, 571, 575-93. doi: 10.1016/j.scitotenv.2016.07.024.

Zhang, S., H. Gao, and B. S. Naz, 2014. Monitoring reservoir storage in Asia from multisatellite remote sensing, Water Resour. Res., 50, doi:10.1002/2014WR015829.

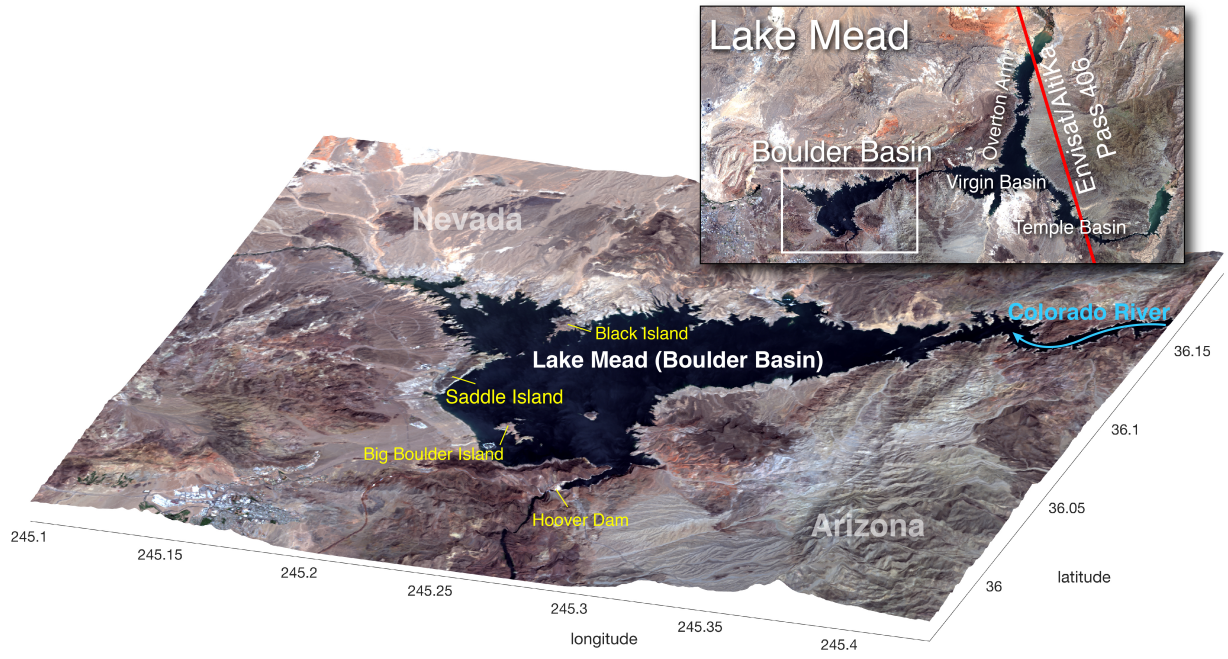

546

547 **Fig. 1**: Geographical information of Lake Mead in the USA and the Boulder Basin aimed in this
548 study. This figure is derived from a Landsat-8 OLI image taken on August 14, 2017.

549

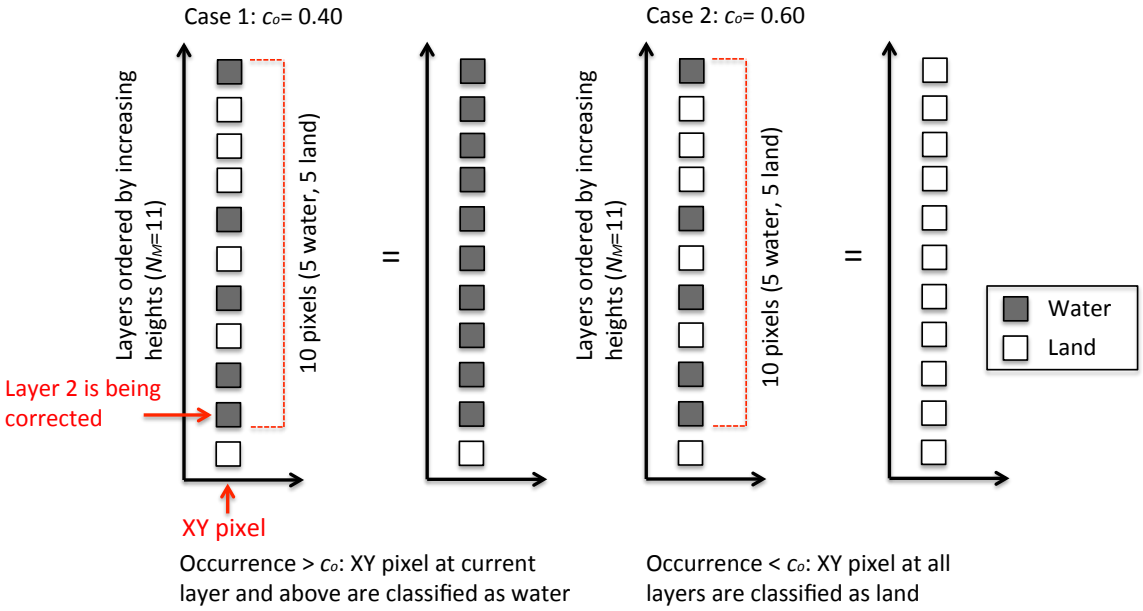

550

551 **Fig. 2:** Example of multi-temporal pixel-based water extent correction as a function of the
552 occurrence coefficient (c_o). In both cases, the occurrence is 0.50.

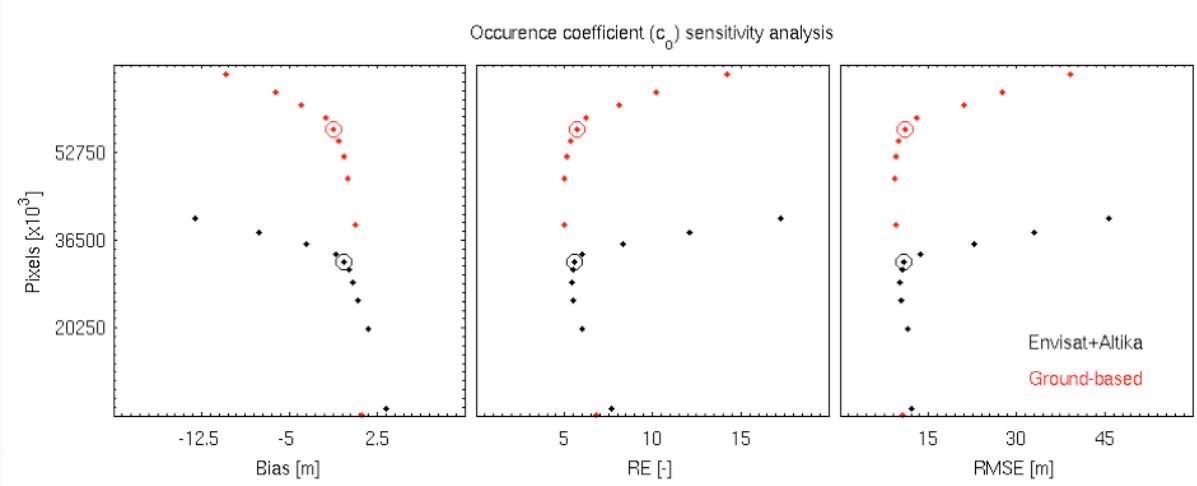

553

554 **Fig. 3:** Bias, RE and RMSE derived from the occurrence coefficient (c_o) sensitivity analysis as a
555 function of the number of pixels used to build satellite-based visible bathymetry. Scatter plots
556 show results from c_o varying from 0.1 to 1 at 0.1 incrementing steps. Circles point to the selected
557 value (c_o=0.5). c_o values increase from the top to the bottom on the vertical axis.

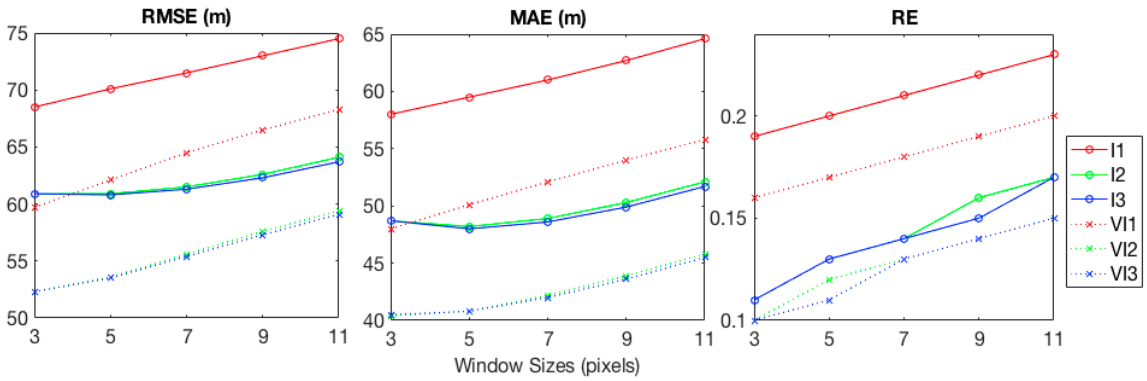

Fig. 4: Sensitivity analysis of moving average window size. The evaluation is shown for six experiments considering the linear interpolation technique.

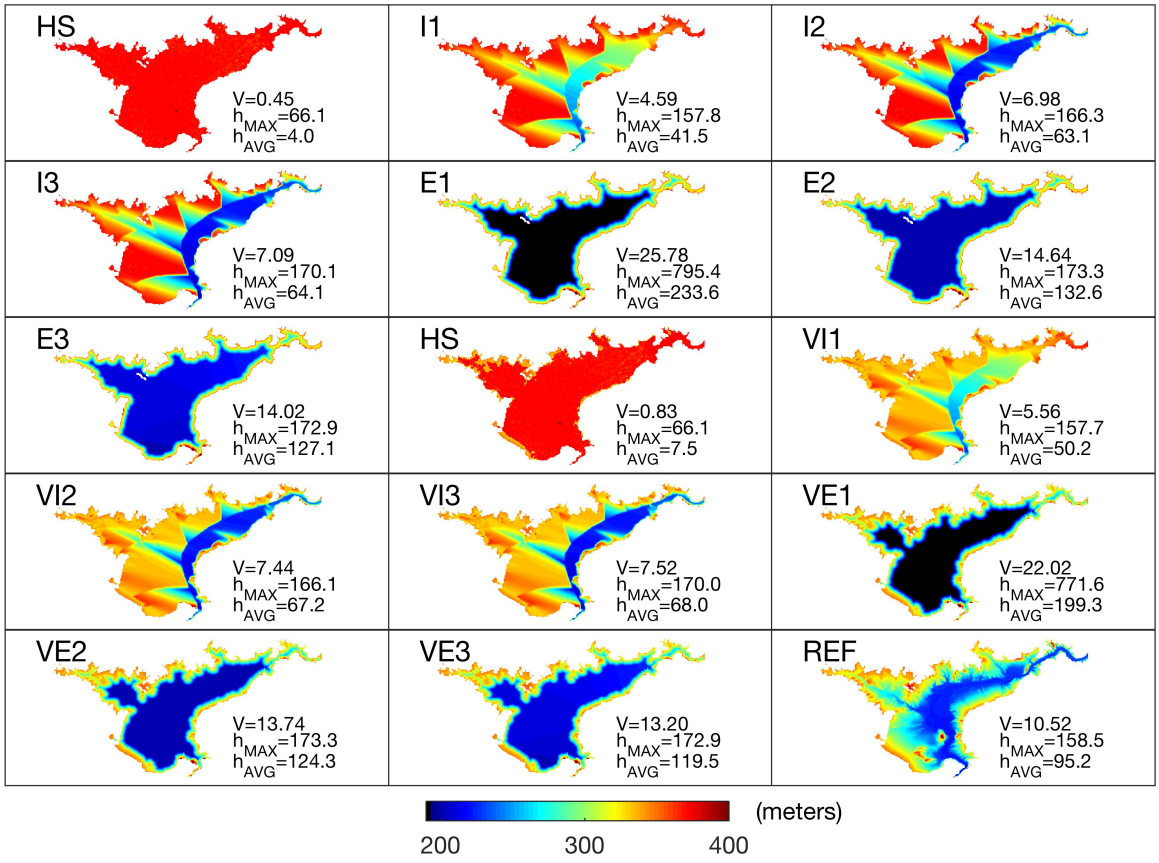

561

562 **Fig. 5:** Bathymetry derived from fourteen methods with increasing data requirement and
563 processing, as listed in Table 1. The observed bathymetry (REF) is also shown for comparison
564 purposes. Volume V is in km^3 and depths h_{MAX} and h_{AVG} are in meters.

565

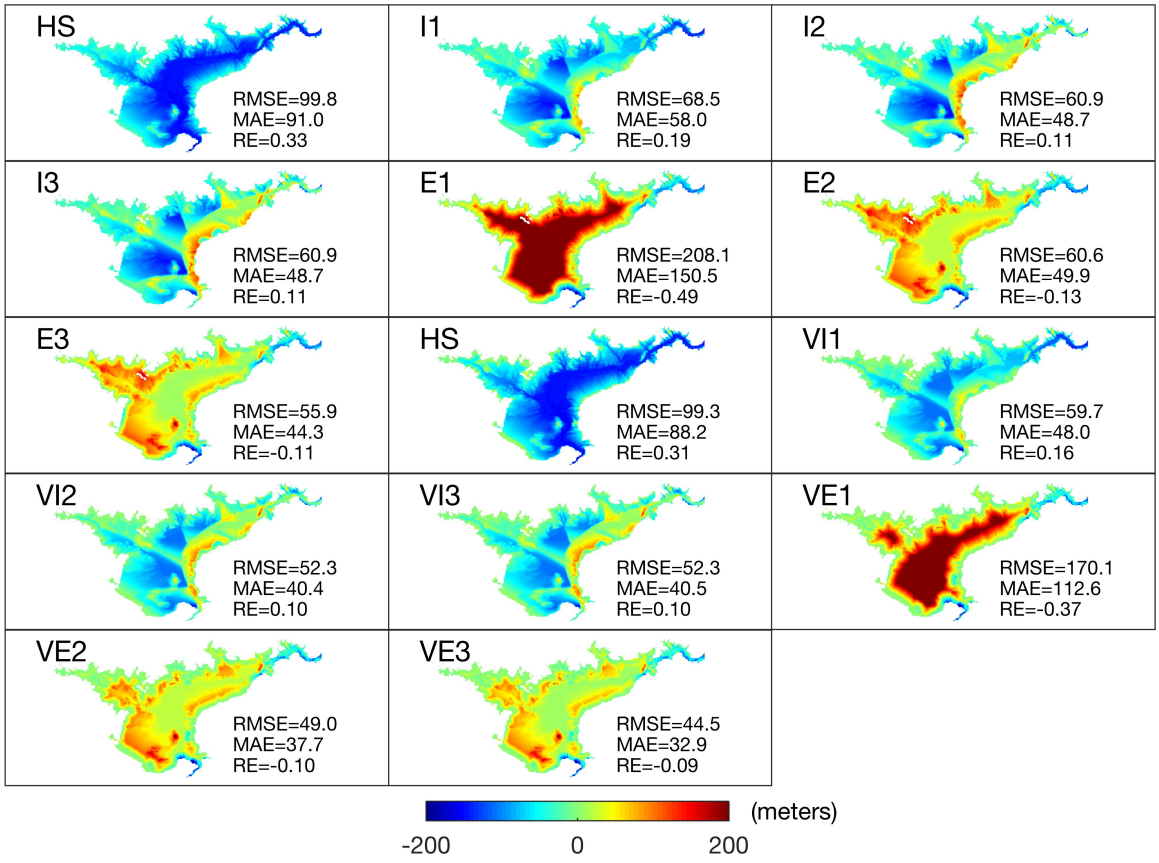

566

567 **Fig. 6:** Difference between bathymetries derived from fourteen methods and the reference (i.e.
568 positive values represent overestimated depths), as listed in Table 1. RMSE and MAE values are
569 in meters, and RE is unitless.

570

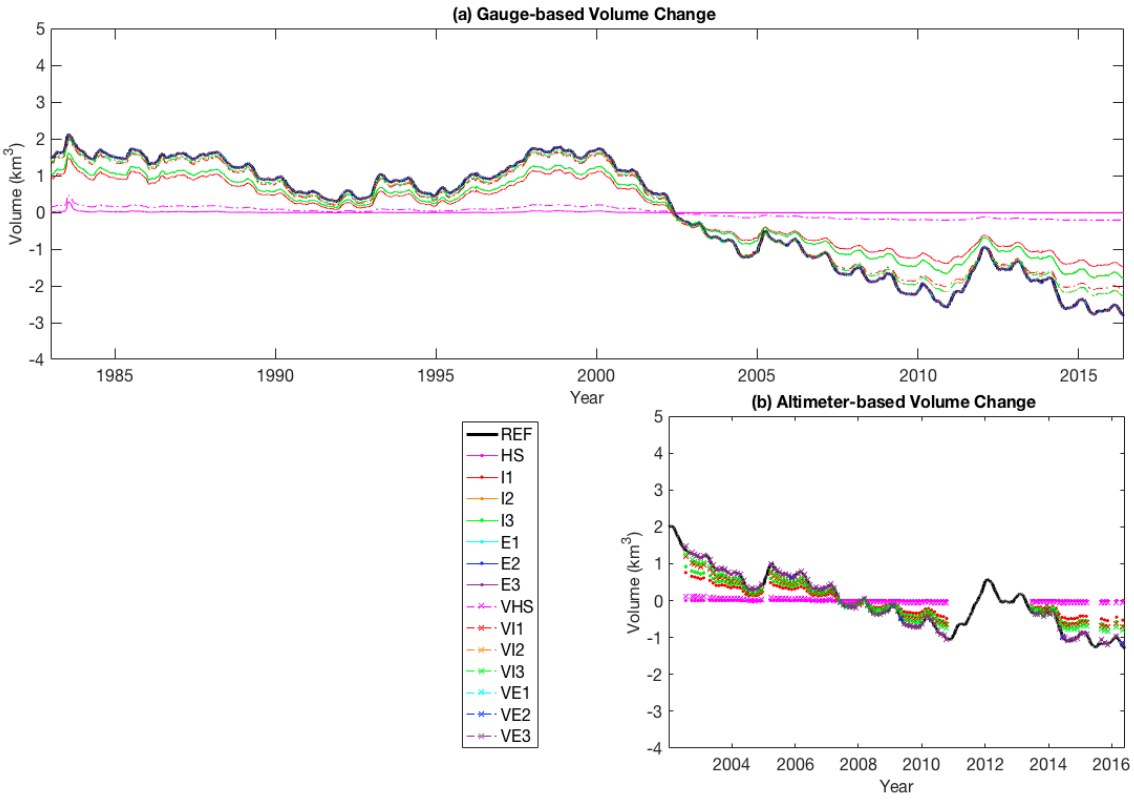

571

572 **Fig. 7:** Water volume variability in Boulder Basin resulting from satellite-based bathymetries
573 combined with (a) ground-based water level observations and (b) radar altimetry data. Ground-
574 based water volume variability is also shown for comparison. Bias [km^3], RMSE [km^3] and
575 standard deviation ratio (Stdev ratio) [-] are provided in Table 2.

576 **Table 1**: Summary of experiments for bathymetry generation.

Experiment	Procedure (data processing)	Data requirement
1 (HS)	-	DEM
2 (I1)	Linear interpolation	DEM
3 (I2)	Linear interpolation (using upstream riverbed elevation and downstream DEM elevation)	DEM; Riverbed elevation
4 (I3)	Linear interpolation (using upstream and downstream riverbed elevations)	DEM; River bed elevation
5 (E1)	Linear extrapolation	DEM
6 (E2)	Linear extrapolation; Flat horizontal bottom using downstream riverbed elevation	DEM; River bed elevation
7 (E3)	Linear extrapolation; Bottom constrained with flat surface using interpolation of upstream and downstream riverbed elevation	DEM; River bed elevation
8 (VHS)	Visible bathymetry	DEM; Water level and extent time series
9 (VI1)	Linear interpolation; Visible bathymetry	DEM; Water level and extent time series
10 (VI2)	Linear interpolation (using upstream riverbed elevation and downstream DEM elevation); Visible bathymetry	DEM; Riverbed elevation; Water level and extent time series
11 (VI3)	Linear interpolation (using upstream and downstream riverbed elevations); Visible bathymetry	DEM; Riverbed elevation; Water level and extent time series
12 (VE1)	Linear extrapolation; Visible bathymetry	DEM; Water level and extent time series
13 (VE2)	Linear extrapolation Bottom constrained with flat horizontal surface using downstream riverbed elevation; Visible bathymetry	DEM; Riverbed elevation; Water level and extent time series
14 (VE3)	Linear extrapolation (bottom constrained with flat surface using interpolation of upstream and downstream riverbed elevation); Visible bathymetry	DEM; Riverbed elevation; Water level and extent time series

577

578

Table 2: Bias [km^3], RMSE [km^3] and standard deviation ratio (Stdev ratio) [-] of water volume variability derived from ground-based and satellite-based water levels combined with 14 bathymetric estimates.

	Ground-based volume change			Satellite-based volume change		
	Bias	RMSE	Stdev ratio	Bias	RMSE	Stdev ratio
HS	-8.24	1.44	0.02	-6.73	0.70	0.00
I1	-5.60	0.61	0.59	-4.97	0.36	0.48
I2	-3.51	0.48	0.68	-3.02	0.28	0.60
I3	-3.42	0.47	0.68	-2.93	0.28	0.60
E1	10.00	0.00	1.00	10.00	0.03	0.99
E2	4.12	0.00	1.00	4.13	0.03	0.99
E3	3.51	0.00	1.00	3.51	0.03	0.99
VHS	-8.04	1.31	0.10	-6.67	0.65	0.07
VI1	-5.15	0.21	0.87	-4.98	0.21	0.72
VI2	-3.47	0.16	0.91	-3.35	0.16	0.79
VI3	-3.40	0.15	0.91	-3.27	0.16	0.79
VE1	10.00	0.01	1.01	10.00	0.03	1.00
VE2	3.21	0.01	1.01	3.21	0.03	1.00
VE3	2.68	0.01	1.01	2.67	0.03	1.00